Electronic Supplementary Information

Highly conductive and bendable gold networks attached on intertwined cellulose fibers for output controllable power paper

Yan Zhang,[ab] Hongmei Yang,[a] Kang Cui,[a] Lina Zhang,*[c] Jinmeng Xu,[a] Hong Liu[d] and Jinghua Yu*[a]

[a] *School of Chemistry and Chemical Engineering, University of Jinan, Jinan 250022, China. E-mail: ujn.yujh@gmail.com*

[b] *School of Materials Science and Engineering, University of Jinan, Jinan 250022, China.*

[c] *Shandong Provincial Key Laboratory of Preparation and Measurement of Building Materials, University of Jinan, Jinan 250022, China. E-mail: zhanglina818@126.com*

[d] *Institute for Advanced Interdisciplinary Research, University of Jinan, Jinan 250022, China*

Content

Regents and materials

Preparation of AuNPs seeds

In-situ synthesis of PB film

The influence of AuNPs size on the conductivity of paper-based electrodes

Morphology characterization

Electric performance of power paper

Table S1

Table S2

Table S3

Fig. S1

Fig. S2

Fig. S3

Fig. S4

Fig. S5

Fig. S6

Fig. S7

Fig. S8

Fig. S9

Fig. S10

Fig. S11

References

Regents and materials

Whatman chromatography paper (grade 2 CHR) purchased from GE Healthcare Worldwide (Shanghai, China) was utilized as the substrate for the assembly of paper device. Pyrrole monomer obtained from Aladdin (China) was twice distilled prior to use. Tris(2,2'-bipyridine)dichlororuthanium(II)hexahydrate was obtained from Aladdin Chemical Reagent Co. Ultrapure water (≥18.25 MΩ cm) produced from a Lichun water purification system (Jinan, China) was utilized throughout the experiments.

Preparation of AuNPs seeds

The AuNPs seeds solution was synthesized according to previous reported method via the simple reduction of $HAuCl_4$.[1] Briefly, 50 mL $HAuCl_4$ (0.25 mM) was firstly heated to 90 °C and kept for 2 min. Then 3.0 mL of freshly prepared 34 mM trisodium citrate was added. After heated for 10 min, the color of the solution turned wine red, suggestting the successfully preparation of the AuNPs seeds solution.

In-situ synthesis of PB film

The electropolymerization of PB was conducted by applying a constant potential of 0.4 V for 1200 s. A freshly prepared aqueous solution containing 2.5 mM $K_3[Fe(CN)_6]$ and $FeCl_3$, 0.1 M HCl, and 0.1 M KCl was applied as the electrolyte. After deposition, the as-prepared 3D PB films with a sheet of paper thickness were dried at 100 °C for 8 h after being thoroughly washed, and stored in a dark environment shielded from light.

The influence of AuNPs size on the conductivity of paper-based electrodes

Paper-based electrodes (Samples a-c) functionalized by AuNPs of different size have been fabricated as illustrated in Fig. S6 and Table S2. Obviously, it could be found that sample a (Fig. S6a_1-S6a_3) coated with 160-200 nm gold nanoparticles has the best surface uniformity and exhibits the best conductivity in both horizontal and vertical directions. As the particle size of the AuNPs increases (Samples b and c), the surface uniformity deteriorates (Fig. S6b_1-S6b_3 and Fig. S6c_1-S6c_3), accompanied by a decrease in conductivity (Table S2). The reason is that AuNPs with increased particle size can not completely penetrate into the interior of the paper fibers, which in turn affects the formation of continuous gold network structures. As a consequence, paper-based electrodes functionalized by AuNPs with larger size and lower density distribution, exhibit unsatisfactory electrical performance. Summarily, benefiting from the smaller size of AuNPs compared with the pores of the cellulose paper, high density and uniformly dispersed AuNPs with 160-200 nm on the cellulose fiber surfaces, a continuous and dense conductive gold architecture was obtained in this work, exhibiting enhanced electrical performance. Therefore, to construct a highly conductive paper-based electrode, it is preferable to employ AuNPs with smaller size for modification. Furthermore, the higher density of AuNPs distribute, the better conductivity of the electrodes display.

Morphology characterization

The successful electropolymerization of PB film on cellulose paper was confirmed by its obvious color change from white to blue.[2,3] In contrast to raw paper (Fig. 2a), a homogeneous and dense PB film was deposited onto the cellulose surface, as the typical SEM images described (Fig. S9a-c). Moreover, the energy dispersive spectroscopy (EDS) mapping analysis were carried out to investigate the elemental distribution, as revealed in Fig. S9e-j. Obviously, it could be seen that C, N, O, K, and Fe elements were evenly distributed on the cellulose surface. Notably, because of its unique 3D porous structure of paper matrix, PB film also could be formed in the interior framework of paper fibers, thereby the forming PB film having the same thickness as the paper sheet. Hence the cross-sectional view (Fig. S9d) of the product and corresponding EDS mapping images (Fig. S9k-p) characterization were performed. The analytical results were agreed well with the prediction, demonstrating successful coating and uniform distribution of PB film on the cellulose paper framework.

Electric performance of power paper

The half reactions of $Mg/Mg^{2+}$and PW/PB are shown in Equation (S1) - (S2)

$$Mg - 2e^- \rightarrow Mg^{2+} \quad \text{(S1)}$$

$$Fe[Fe(CN)_6]^- \text{ (PB)} + e^- \rightarrow Fe[Fe(CN)_6]^{2-} \text{ (PW)} \quad \text{(S2)}$$

The bleached device recovered its blue color after being oxidized by ClO^-; the corresponding charging process could be described by the following reaction[4]:

$$2Fe[Fe(CN)_6]^{2-} \text{ (PW)} + ClO^- + 2H^+ \rightarrow 2Fe[Fe(CN)_6]^- \text{ (PB)} + Cl^- + H_2O \quad \text{(S3)}$$

Table S1 Sheet resistance comparison of previous reported paper-based materials and fabricated porous gold conductive track.

Species	Materials	Preparing methods	Sheet resistance (Ω sq^{-1})	Reported time	Ref.
Carbon materials	Conductive graphene patterns	Inkjet reduction method	600	2015	5
	Graphene-on-paper	Chemical vapor deposition and dry-transfer	445	2016	6
	Nanostructured reduced graphene coated oxide cellulose fibers paper	Coating and reduction reaction	210	2014	7
	Carbon nanotube film	Blade-coated method	50	2010	8
	Carbon nanotube conductive paper	Coating method	10	2009	9
	Carbon nanotube/bacterial nanocellulose paper	Coating process	7	2012	10
	Reduced graphene oxide paper	Freeze-drying method	0.65	2015	11
Conductive polymers	Polypyrrole incorporated in paper	Gas-phase polymerization	40 ± 1	2016	12
	Polypyrrole modified paper	“Pen-writing” method	17	2014	13
	Polypyrrole-coated paper	Soak and polymerization method	4.5	2013	14
	Freestanding bacterial cellulose–polypyrrole nanofibres paper	Vacuum-filtering method	4.37	2014	15

Composites	Graphite/polyaniline networks	Pencil-drawing and electrodeposition	32.3	2013	16
	Reduced graphene oxide–sulfur composite	Synchronously reducing and assembling	25.9	2016	17
	Single wall carbontube/active carbon and Ag nanowire	Inkjet-printing	8	2016	18
	Au/polyvinyl alcohol/polyaniline-coated paper	Deposition and electropolymerization	7	2012	19
	Free-standing reduced graphene oxide/polypyrrole/ cellulose hybrid papers	In situ polymerization and chemical reduction	1.7	2017	20
Metals and metal oxides	Metallic single-walled carbon nanotubes/AuNP hybrid film on mixed cellulose ester	Ambient filtration	37	2015	21
	Copper nanowire transparent conducting electrode	Plasma-enhanced chemical vapor deposition process	32	2011	22
	Silver nanowires networks on nanopaper	Filtration method	12	2014	23
	Tin doped indium oxide-coated paper	Sputtering method	12	2013	24
	Al deposited paper	Chemical solution process	0.25	2013	25
	Porous gold conductive track	Double bottom-up growth method	1.6	--	This work

Table S2 Conductivity comparison of paper-based electrodes modified with AuNPs of different size.

Sample	AuNPs size distribution (nm)	Density distribution	Horizontal sheet resistance ($\Omega \cdot sq^{-1}$)	Vertical conductivity ($S \cdot cm^{-1}$)
a	160-200	High	1.60	44.58
b	450-550	Moderate	3.52	2.37
c	250-2000	Low	57.8	0.019

Table S3 Power density comparison of different power devices.

Power devices	Power density ($mW\ cm^{-2}$)	Ref.
Self-feeding paper based biofuel cell	0.87	26
Paper-based biofuel cells using printed porous carbon electrodes	0.12	27
Enzymatic biofuel cells based on nitrogen-doped hollow carbon nanospheres functionalized electrode	0.325±0.0006	28
Photoelectrochemical fuel cells	13.34	29
Microbial fuel cells based on three dimensional graphene-based frameworks	897.1	30
Single-use paper-based hydrogen fuel cells	103.20	31
Output controllable power paper	11.58	This work

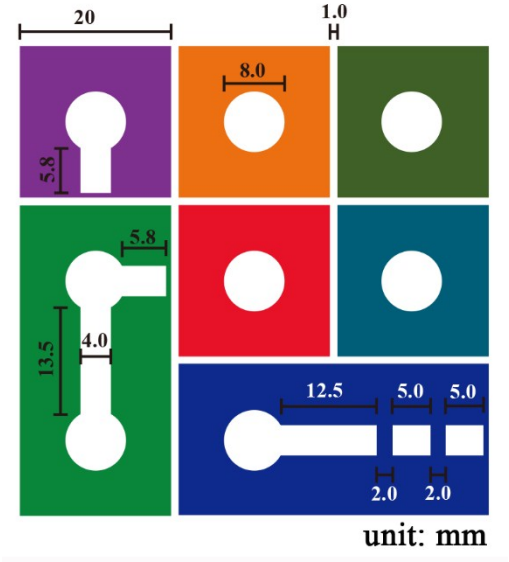

Fig. S1 The schematic representation of the power paper device designed with Adobe Illustrator CS4.

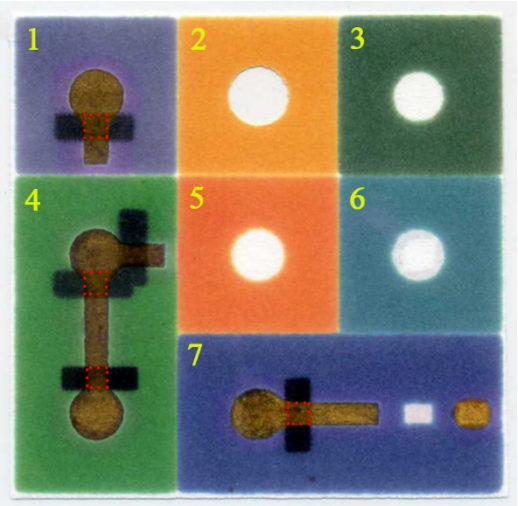

Fig. S2 Photograph of integrated paper microfluidic platform after double bottom-up growth of AuNPs and secondary wax-printing. The circle-shaped hole cut by a punch plier was used to place Mg sheet. Red dotted areas are hydrophobic gold wires. The numbers refer to hydrophobic regions defined by colored wax.

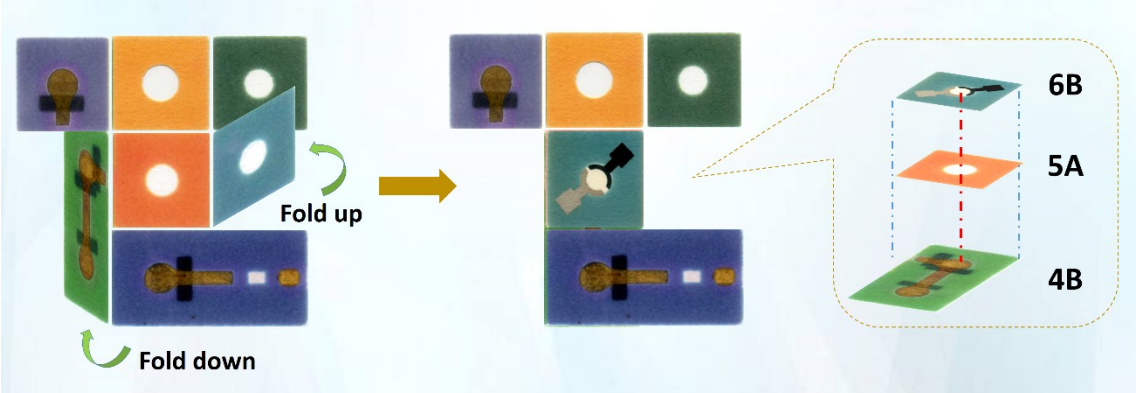

Fig. S3 The schematic folding step of paper device for the electroploymerization of PB film. The number is consistent with the area defined in Fig. S2. A and B refer to the front and back sides of the paper respectively.

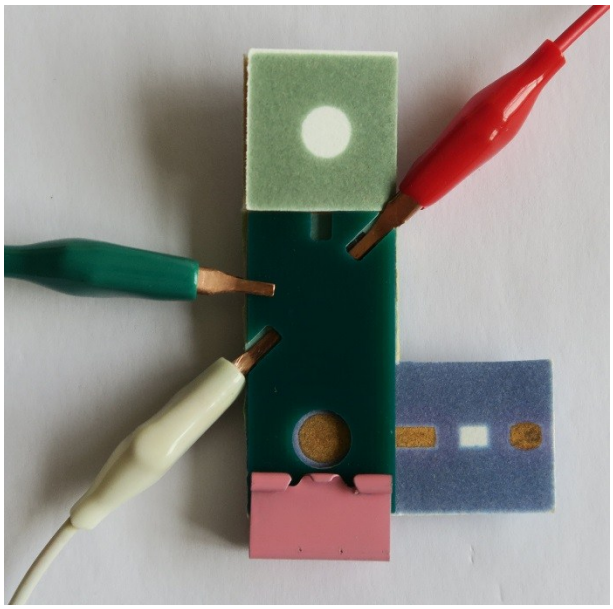

Fig. S4 Photographs of fabricated integrated paper microfluidic platform for electroploymerization of PB film.

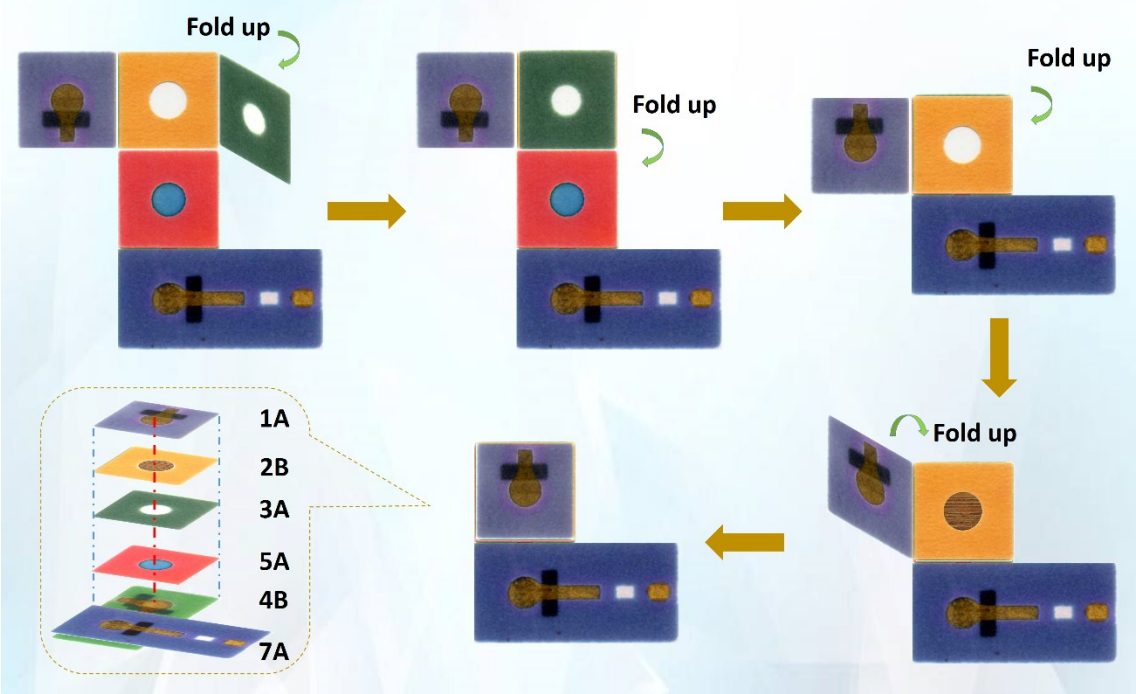

Fig. S5 The schematic folding step of power paper device. The number is consistent with the area defined in Fig. S2. A and B refer to the front and back sides of the paper respectively.

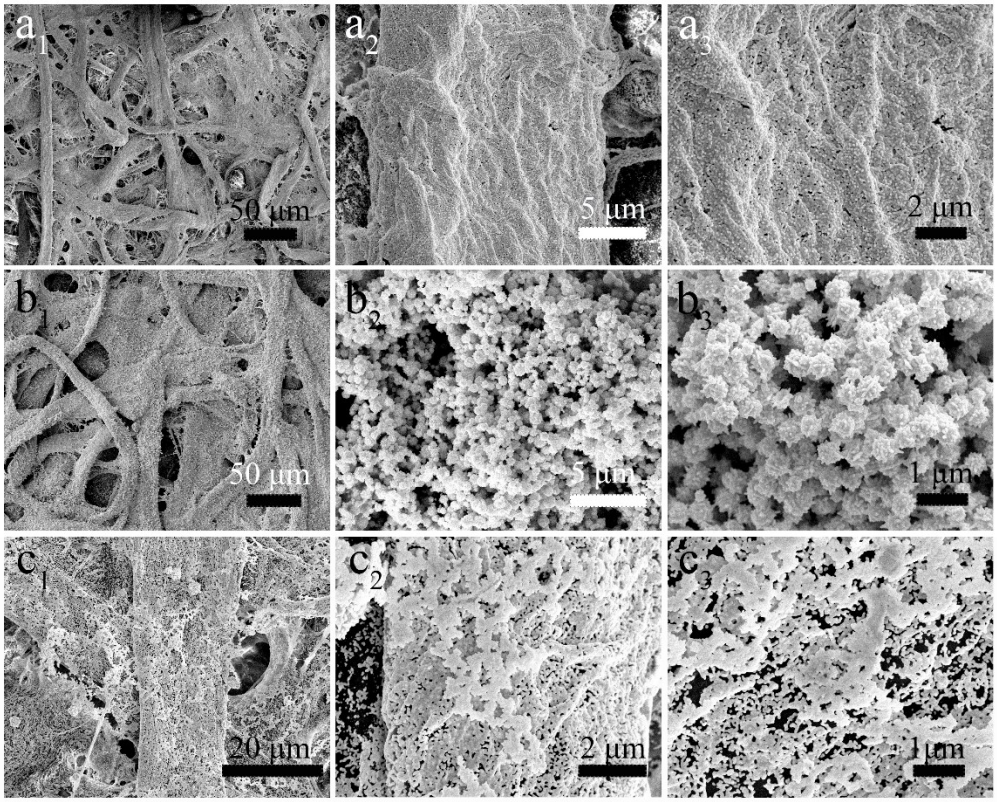

Fig. S6 Representative SEM images of paper-based electrodes modified with AuNPs of different size (a_i-c_i) at different magnification (i=1-3).

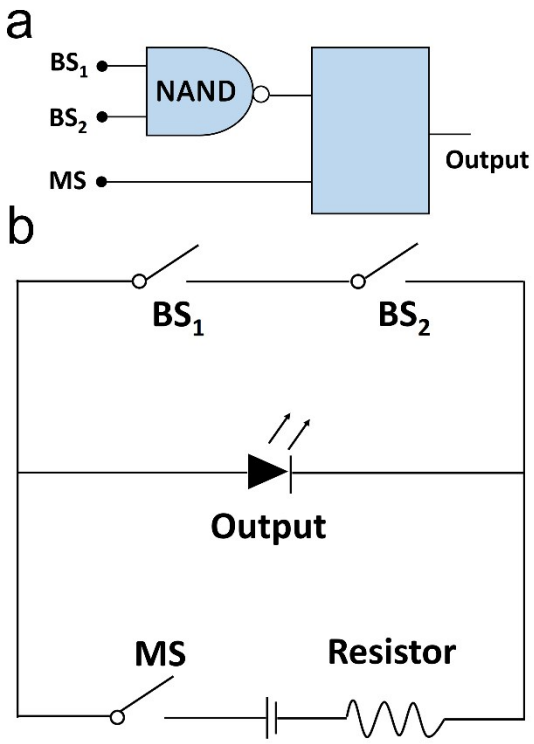

Fig. S7 NAND logic gate. (a) Proposed symbol for NAND logic gate. MS: main switch; BS: branch switch. (b) A physical circuit for fabricated paper-based NAND logic gate.

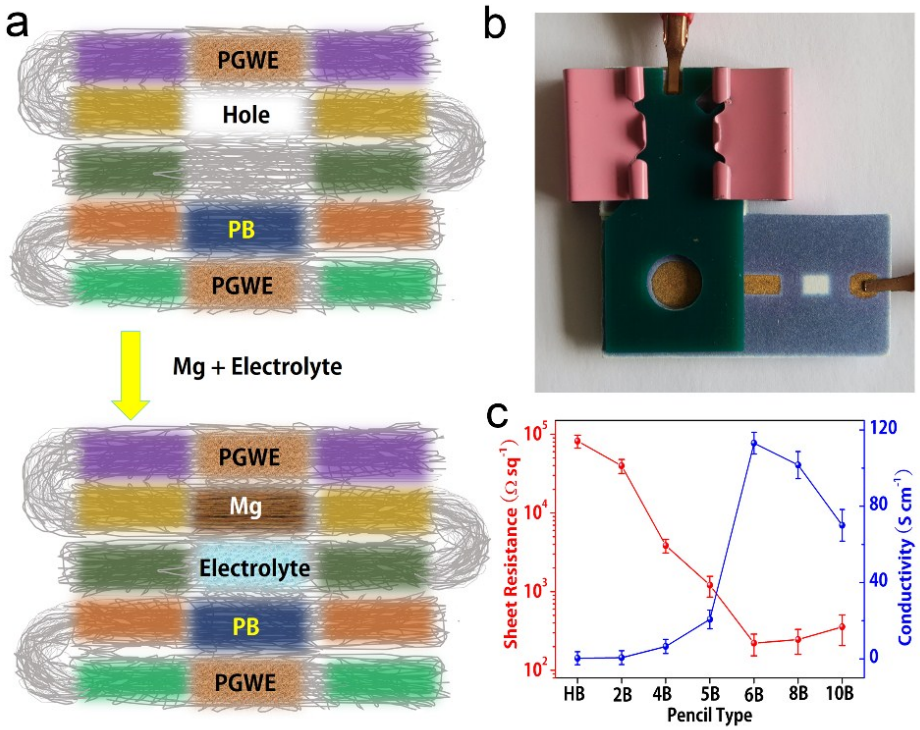

Fig. S8 Overview of the fully integrated paper microfluidic platform and electrical properties of graphite layer drawn on paper. (a) Schedule of the fully integrated paper microfluidic platform from model to power paper. (b) Photograph of the constructed fully integrated paper microfluidic platform. (c) Sheet resistance and electrical conductivity of the pencil-drawing graphite layer on paper with respect to various pencil types.

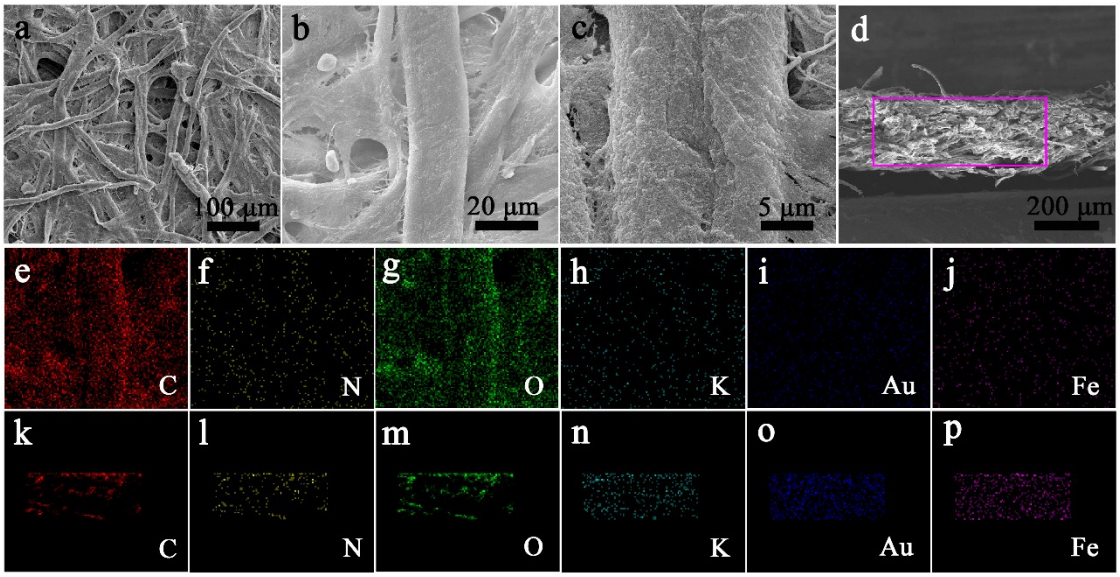

Fig. S9 Morphological and composition characterizations of the as-prepared 3D PB film. (a-c) SEM images of electropolymerized 3D PB film on porous paper. (d) Cross-sectional SEM image of 3D PB film. (e-p) The EDS elemental mapping images of 3D PB film of the corresponding surface (c) and cross-sectional (d) image, demonstrating the homogeneous distribution of: (e, k) carbon, (f, l) nitrogen, (g, m) oxygen, (h, n) potassium, (i, o) gold, and (j, p) iron elements.

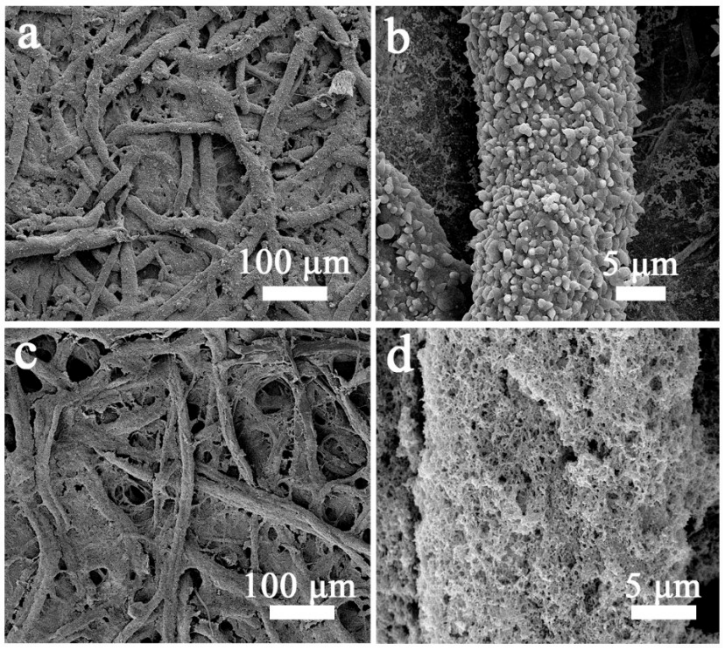

Fig. S10 Typical low- and high-magnification SEM images of electropolymerized (a, b) PPy film and (c, d) PANI network.

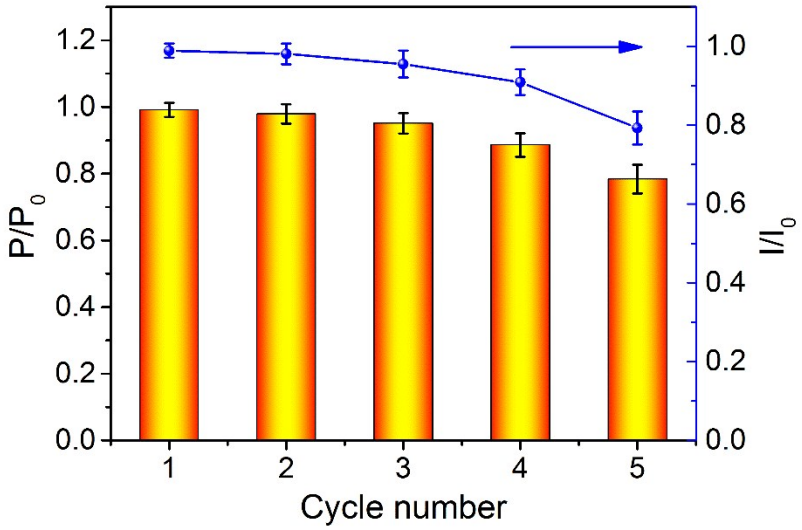

Fig. S11 Performance of power paper. Repeated rechargeability examination of the fabricated power paper by simply disconnecting PB and Mg in 1 M KCl, 0.025 M ClO^-, and 0.1 M phosphate buffer. P: power density. And in-situ gray intensity measurement of deposited PB film under repeated discharging and charging cycles.

References

1. H. Yang, Y. Zhang, L. Li, L. Zhang, F. Lan, J. Yu. *Anal. Chem.*, 2017, **89**, 7511-7519.
2. N. Zhu, S. Han, S. Gan, J. Ulstrup, Q. Chi, *Adv. Funct. Mater.*, 2013, **23**, 5297-5306.
3. Y. Huang, M. Xie, J. Zhang, Z. Wang, Y. Jiang, G. Xiao, S. Li, L. Li, F. Wu, R. Chen, *Nano Energy*, 2017, **39**, 273-283.
4. H. Zhang, Y. Yu, L. Zhang, Y. Zhai, S. Dong, *Chem. Sci.*, 2016, **7**, 6721-6727.
5. Y. Su, S. Jia, J. Du, J. Yuan, C. Liu, W. Ren, H. Cheng, *Nano Research*, 2015, **8**, 3954-3962.
6. H. Zhu, Z. Fang, Z. Wang, J. Dai, Y. Yao, F. Shen, C. Preston, W. Wu, P. Peng, N. Jang, Q. Yu, Z. Yu, L. Hu, *ACS Nano*, 2016, **10**, 1369-1377.
7. L. Liu, Z. Niu, L. Zhang, W. Zhou, X. Chen, S. Xie, *Adv. Mater.*, 2014, **26**, 4855-62.
8. L. Hu, H. Wu, F. La Mantia, Y. Yang, Y. Cui, *ACS Nano*, 2010, **4**, 5843-5848.
9. L. Hu, J.W. Choi, Y. Yang, S. Jeong, F. La Mantia, L.-F. Cui, Y. Cui, *Proc. Nat. Acad. Sci.*, 2009, **106**, 21490-21494.
10. Y.J. Kang, S.-J. Chun, S.-S. Lee, B.-Y. Kim, J.H. Kim, H. Chung, S.-Y. Lee, W. Kim, *ACS Nano*, 2012, **6**, 6400-6406.
11. C. Wang, X. Wang, Y. Yang, A. Kushima, J. Chen, Y. Huang, J. Li, *Nano Lett.*, 2015, **15**, 1796-1802.
12. M. Santhiago, J. Bettini, S.R. Araújo, C.C.B. Bufon, *ACS Appl. Mater. Interfaces*, 2016, **8**, 10661-10664.
13. H. Jia, J. Wang, X. Zhang, Y. Wang, *ACS Macro Lett.*, 2014, **3**, 86-90.
14. L. Yuan, B. Yao, B. Hu, K. Huo, W. Chen, J. Zhou, *Energy Environ. Sci.*, 2013, **6**, 470-476.
15. S. Li, D. Huang, J. Yang, B. Zhang, X. Zhang, G. Yang, M. Wang, Y. Shen, *Nano Energy*, 2014, **9**, 309-317.
16. B. Yao, L. Yuan, X. Xiao, J. Zhang, Y. Qi, J. Zhou, J. Zhou, B. Hu, W. Chen, *Nano Energy*, 2013, **2**, 1071-1078.
17. J. Cao, C. Chen, Q. Zhao, N. Zhang, Q. Lu, X. Wang, Z. Niu, J. Chen, *Adv. Mater.*, 2016, **28**, 9629-9636.
18. K.-H. Choi, J. Yoo, C.K. Lee, S.-Y. Lee, *Energy Environ. Sci.*, 2016, **9**, 2812-2821.
19. L. Yuan, X. Xiao, T. Ding, J. Zhong, X. Zhang, Y. Shen, B. Hu, Y. Huang, J. Zhou, Z.L. Wang, *Angew. Chem.*, *Int. Ed.*, 2012, **51**, 4934-4938.
20. C. Wan, Y. Jiao, J. Li, *J. Mater. Chem. A*, 2017, **5**, 3819-3831.
21. B. Guntupalli, P. Liang, J.-H. Lee, Y. Yang, H. Yu, J. Canoura, J. He, W. Li, Y. Weizmann, Y. Xiao, *ACS Appl. Mater. Interfaces*, 2015, **7**, 27049-27058.
22. Y. Ahn, Y. Jeong, D. Lee, Y. Lee, *ACS Nano*, 2015, **9**, 3125-3133.
23. H. Koga, M. Nogi, N. Komoda, T. T. Nge, T. Sugahara, K. Suganuma, *NPG Asia Mater.*, 2014, **6**, e93.
24. L. Hu, G. Zheng, J. Yao, N. Liu, B. Weil, M. Eskilsson, E. Karabulut, Z. Ruan, S. Fan, J.T. Bloking, M.D. McGehee, L. Wagberg, Y. Cui, *Energy Environ. Sci.*, 2013, **6**, 513-518.
25. H.M. Lee, S.-Y. Choi, A. Jung, S.H. Ko, *Angew. Chem.*, 2013, **125**, 7872-7877.
26. C.W. Narvaez Villarrubia, F. Soavi, C. Santoro, C. Arbizzani, A. Serov, S. Rojas-Carbonell, G. Gupta, P. Atanassov. *Biosens. Bioelectron.*, 2016, **86**, 459-465

27. I. Shitanda, S. Kato, Y. Hoshi, M. Itagaki, S. Tsujimura. *Chem. Commun.*, 2013, **49**, 11110-11112.
28. L.L. Wang, H.H. Shao, W.J. Wang, J.R. Zhang, J.J. Zhu. *Nano Energy*, 2018, **44**, 95-102.
29. H. Zhang, Y. Yu, L. Zhang, Y. Zhai, S. Dong. *Chem. Sci.*, 2016, **7**, 6721-6727.
30. M. Chen, Y. Zeng, Y. Zhao, M. Yu, F. Cheng, X. Lu, Y. Tong. *J. Mater. Chem. A*, 2016, **4**, 6342-6349.
31. J.P. Esquivel, J.R. Buser, C.W. Lim, C. Domínguez, S. Rojas, P. Yager, N. Sabaté. *J. Power Sources*, 2017, **342**, 442-451.